2

CONF-890811--25

SAND88-2504C
To be presented at the Ninth
Symposium on Detonation
8/28-9/1/89, Portland, OR

COMPRESSIVE COMBUSTION OF GRANULAR MATERIALS INDUCED BY LOW-VELOCITY IMPACT

M. R. Baer and J. W. Nunziato

Fluid and Thermal Sciences Department
Sandia National Laboratories
Albuquerque, New Mexico, 87185, USA

SAND--89-2504C

DE89 014900

A reactive multiphase mixture model is used to describe the initiation and compressive combustion of granular energetic materials induced by dynamic compaction. Incorporated in this description is a two-step combustion model whereby compressive reaction is initiated by dynamic compaction. Subsequent energy release from the reaction gases evolved during compaction is delayed following an induction rate law based on time-to-reaction experimental data. Given conditions of sufficient energy release and heat transfer, grain burning is initiated when granular surface temperatures exceed decomposition conditions. Model parameters are formulated for the granular explosive HMX and for nitrocellulose-based ball propellants. This model is used to simulate the low-velocity impact experiments of Sandusky and coworkers. Numerical calculations compare well with experimental observations. Details of compaction and combustion behavior are illustrated near the threshold of deflagration-to-detonation transition (DDT).

INTRODUCTION

The modes of flame spread and the transition from deflagration to detonation (DDT) in gas-permeable reactive granular materials are known to involve a variety of complex thermal/mechanical/chemical processes. To gain a fundamental understanding of these processes, several experimental studies have focused on various aspects of a DDT event. Bernecker, et al.[1,2] studied accelerated combustion in confined columns of granular explosives and propellants and proposed mechanisms for DDT based on wave trajectory information. Most importantly, it has been shown that compaction of the granular reactant plays a major role in the combustion process. In view of this result, a number of subsequent studies investigated the nature of mechanically induced ignition and reaction using low level impact experiments. The projectile impact studies of Green, et al.[3], demonstrated that compaction, by itself, triggers a combustion event that readily accelerates to detonation provided that a certain level of porosity exists. In similar studies, Sandusky and coworkers[4,5] showed that rapid distortion of the granular material at a compaction front induces compressive reaction with a delay in energy release. Reaction product gases assist the mechanical loading of the granular material and strengthen the compaction wave. McAfee and Campbell[6] conducted piston impact experiments that revealed multiple compaction fronts that form as a result of the interaction of combustion and the loss of lateral wall confinement. In all of these studies, low-velocity impact produces low amplitude compressive waves that are insufficient to cause direct shock initiation, and yet, DDT is observed. It is now recognized that 'hot-spot' reaction during compaction is the key that links the combustion modes of convective burning and detonation.

Much progress has been made toward the development of reactive multiphase mixture models describing deflagration-to-detonation transition in granular materials. A review and survey of the various modeling approaches is beyond the scope of this work and the interested reader is referred to the works

---

of Baer and Nunziato,[7] Butler and Krier,[8] Kooker,[9] Kim[10] and the various works on DDT which appeared in the Eight Symposium (International) on Detonation.[11] Much effort has been devoted to the determination of appropriate constitutive models and in providing verification data for modeling. Indeed, the interactive use of numerical models and experimental data calibrates modeling quantitatively and assists in elucidating the operative mechanisms in experiments.

Although existing models are well-founded from a thermodynamic and mechanical point of view and the concept of 'hot-spot' formation is well accepted, little progress has been made in defining the precise microscopic physical mechanisms that control nucleation, growth and coalescence of 'hot-spots'. Moreover, chemical mechanisms and rates are not well defined for conditions at high dynamic pressure. Given limited experimental time-to-reaction data relevant at the conditions of high strain rate deformation, a phenomenological combustion description for 'hot-spot' decomposition and grain burning is used in this study.

In the sections that follow, we review the multiphase mixture model for energetic granular materials with emphasis on the combustion description. Appropriate model inputs are defined and numerical calculations are carried out to model the low-velocity impact experiments conducted by Sandusky, et al.[4,5] investigating Class D HMX and nitrocellulose-based ball propellants. These reactants are well characterized and experimental data exist to construct appropriate constitutive models for compaction and combustion. Additionally, the ball propellants are ideally suited for modeling since these materials consist of uniform spherical particles that deform plastically during compaction whereas HMX crystals fracture during loading.

REACTIVE MULTIPHASE MIXTURE MODEL

In this model, chemically reacting mixtures are assumed to consist of two phases: the solid granular reactant ($a = s$) and the interstitial gas products ($a = g$). Associated with each phase is a set of state variables: phase velocity v_a, material density ρ_a, pressure p_a, total energy $E_a = e_a + v_a^2/2$, internal energy e_a and volume fraction ϕ_a. In one dimension, the reactive multiphase equations are written in conservation form as:[7]

Conservation of Mass

$$\frac{\partial}{\partial t}(\phi_a \rho_a) + \frac{\partial}{\partial x}(\phi_a \rho_a v_a) = c_a^+, \qquad (1)$$

Conservation of Momentum

$$\frac{\partial}{\partial t}(\phi_a \rho_a v_a) + \frac{\partial}{\partial x}(\phi_a \rho_a v_a^2 + \phi_a p_a) = m_a^+. \qquad (2)$$

Conservation of Energy

$$\frac{\partial}{\partial t}(\phi_a \rho_a E_a) + \frac{\partial}{\partial x}((\phi_a \rho_a E_a + \phi_a p_a) v_a) = e_a^+. \qquad (3)$$

Compaction Equation

$$\frac{\partial \phi_s}{\partial t} + v_s \frac{\partial \phi_s}{\partial x} = \frac{\phi_s \phi_g}{\mu_c}(p_s - p_g - \beta_s) + \frac{c_s^+}{\rho_s}, \qquad (4)$$

where c_s^+, m_s^+ and e_s^+ represent phase interactions of mass, momentum and energy. These phase interaction terms account for the chemical reactions, the interphase drag, and the interphase heat transfer. Constitutive equations for the interphase drag and heat transfer are given elsewhere.[7]

In this description, independent equations of state for each phase are admissable given of the form:

$$p_a = p_a(\rho_a, e_a). \qquad (5)$$

For the gas phase, the Jones-Wilkins-Lee equation of state[12] is used and for the solid phase a thermoelastic state relationship[13] is fit to available shock Hugoniot data[14,15].

Volume fraction changes are described by the compaction equation (4) and, the phases occupy all of the total volume, thus:

$$\phi_s + \phi_g = 1. \qquad (6)$$

Notice that compaction is rate-dependent and is driven by pressure differences. The intragranular stress is denoted as β_s and reflects distortion of the solid granular reactant. The compaction viscosity μ_c controls the rate at which the volume fraction adjusts toward pressure equilibrium. Quasi-static[16,17] and dynamic compaction data[18] are used with compaction shock jump conditions defining the intragranular stress and the compacted solid volume fraction. In this work, wall friction effects and granular shear stresses are neglected.

In terms of multiphase mixtures, the reaction rate includes the effect of compressive reaction in the mass exchange c_s^+. Thus, the mass exchange combines the effects of compaction-induced 'hot-spot' combustion and grain burning:

$$c_s^+ = -\frac{\rho_s(\phi_s - \phi_s^\circ)}{\tau_H} - \rho_s \langle \frac{S}{V} \rangle a p_g^n H(T_s - T^*) = -c_g^+, \qquad (7)$$

where ϕ_s° is the undisturbed solid volume fraction, τ_H is a 'hot spot' reaction time characterizing compaction-induced combustion, $\langle S/V \rangle$ is the specific surface area of the granular reactant, and $a p_g^n$ is the pressure-dependent surface burn

rate[19,20] which is activated by the Heaviside function, $H(T_s - T^*)$. The Heaviside function has a value of one when the granular surface temperature, T_s, exceeds a critical 'ignition' temperature, T^* (corresponding to rapid thermal decomposition[21]), otherwise it is zero.

The first term of this expression applies only to compacted reactant (*i.e.*, $\phi_s > \phi_s^c$) and reflects the effect of compaction-induced combustion. Following experimental observation[4] the reaction time, τ_H, is scaled to the inverse of the square of mixture pressure:

$$\tau_H^{-1} = b p_m^2. \tag{8}$$

The coefficient b is a model parameter determined for each reactant calibrated to replicate the reactive wave characteristics for a specified loading condition. At other impact conditions, this combustion parameter remains fixed.

The second term of Equation (7) represents grain burning and incorporates strand data.[19,20] The specific surface area of the granular reactant is modified by particle burning and by the reduced surface area of pore-collapse during compaction:

$$\left\langle \frac{S}{V} \right\rangle = \frac{6\phi_s}{d_p} \left(\frac{\phi_s^c}{\phi_s} \right)^{\frac{1}{3}} \left(\frac{1-\phi_s}{1-\phi_s^c} \right)^{\frac{2}{3}}, \tag{9}$$

where d_p is the unreacted surface mean particle diameter.

Motivated by experimental observations,[4] the delay of energy release in the 'hot-spot' decomposition gas products is included in the model using a normalized induction time, I. This is mathematically expressed as an evolutionary equation:

$$\frac{\partial I}{\partial t} + v_g \frac{\partial I}{\partial x} = c p_m^2. \tag{10}$$

The heat release in the gas phase, ΔE, is then given by:

$$\Delta E = Q^* + (\Delta E_R - Q^*)\, H(I-1), \tag{11}$$

where Q^* is the energy release during compaction-induced combustion due to 'hot spots' and ΔE_R is the heat of explosion of the reactant. The Q^* is estimated based on the condensed-phase (subsurface reaction) energy release given by Fifer.[22] The parameter c is determined based on experimental time-to-reaction data.[4]

During convective burning, the surface layers of the granular reactant are first ignited. The grain surface temperature, T_s, is determined using a relationship which approximates the heat conduction within particles subjected to convective heat transfer from the hot reaction product gases.[23] The resulting thermal fields are defined by an evolutionary equation, in terms of a surface temperature function ς:

$$\frac{\partial \varsigma}{\partial t} + v_s \frac{\partial \varsigma}{\partial x} = \frac{4\alpha_s B_i}{d_p^2}(T_g - T_s), \tag{12}$$

where T_g is the local bulk gas temperature, α_s is the solid thermal diffusivity and B_i is the Biot modulus (based on the local gas film coefficient h_g, solid thermal conductivity k_s and the particle diameter d_p):

$$B_i = \frac{h_g d_p}{2k_s}. \tag{13}$$

The granular surface temperature is defined as:

$$T_s = \frac{5(3\varsigma + T_s) + B_i T_g}{(5 + B_i)(1 - B_i)} + \frac{B_i \left(T_s - \sqrt{(B_i\varsigma)^2 + 2\varsigma B_i (T_g - T_s)} - B_i\varsigma \right)}{(1 - B_i)}, \tag{14}$$

where T_s is the bulk temperature of the solid phase.

NUMERICAL METHOD

Typical of reactive flow models, the coupling of multiphase transport of mass, momentum and energy with the effects of phase interaction leads to descriptions exhibiting disparate length and time scales. Furthermore, accelerated combustion involves processes that have dominant influences at different times and these processes occur in regions of high gradient or shocks. Thus, an appropriate numerical solution of reactive multiphase flow must recognize and address mathematical stiffness.[24,25] Explicit shock-capture methods, which employ excessive numerical viscosity, can exhibit adequate numerical stability; however, it is usually at the price of accuracy in resolving the combustion physics. Unfortunately, the mathematical structure of multiphase formulations has not been adequately studied for the development of a characteristic-based numerical method.[26] Alternatively, we use a high quality numerical method, extensively studied for this class of reactive flows,[25] that resolves Eulerian multiphase equations with accuracy in time and space.

In this work, one-dimensional numerical solutions of the multiphase flow equations are obtained using an adaptive finite element technique. In this shock-capture method, spatial derivatives are evaluated at Gauss quadrature points and the resulting ordinary differential equations are solved using well-developed ODE software that resolves a large set of highly stiff equations. To incorporate a piston boundary condition, a coordinate transformation is introduced that maps the computational domain to a fixed space.[27] Boundary motion appears explicitly in the conservation equations as grid convective terms. Unphysical numerical dispersion in the hydrodynamic calculations is prevented using a minimal amount of

numerical viscosity incorporated such that numerical truncation and smearing are greatly reduced with grid refinement. An adaptive gridding scheme enhances the accuracy of the numerical solutions by placing fine meshes in regions of extreme gradients. With the adaptive meshing, 50 to 200 computational nodes with eight levels of refinement (each level producing finer meshing) is sufficient for numerical accuracy.

LOW VELOCITY IMPACT OF GRANULAR ENERGETIC MATERIALS

In this section, we use our multiphase reactive flow model to analyze the piston-impact experiments of Sandusky and coworkers.[4,5] Low amplitude impact conditions, similar to those experienced during a DDT event, were investigated using flash X-rays of embedded tracers and probed with high-speed photography, ionization and self-shorting probes, piezoelectric transducers and microwave interferometry. Determination of compaction particle velocities, wave characteristics and wall pressure histories at several locations provide detailed information about the convective and compressive combustion of several confined granular materials; Class D HMX, and ball propellants TS3659 (79.9% NC / 21.6% NG), WC231 (74.8% NC / 25.2% NG) and WC140 (98% NC). Listed in Table 1 are the material properties and combustion parameters for these materials (all transport data are given in Reference 7).

As observed, low-velocity impact produces reaction due to the generation of 'hot spots' during compaction; however, there is a delay time between impact and the detection of intense reaction. After the onset of reaction, the observed growth varied significantly depending on the impact velocity, the confinement and the run distance. In the first comparison of calculation and experimental observation, granular HMX is examined. During quasi-static loading particle fracture occurs;[16] thus a particle diameter of $\sim 100\ \mu$m is used in the reactive flow calculations. Figure 1 displays the observed compaction and burn front trajectories for an impact velocity of 98 m/s in 73% dense Class D HMX. Calculation of this loading condition is shown in Figure 2 as time and distance profiles of solid phase pressure. After impact, a shock-like compaction wave forms that travels into the granular bed at a speed of 430 m/s. After a delay of $\sim 100\ \mu$s, chemical energy is released in the reaction gases produced by the 'hot-spots'. A secondary combustion front then forms and a ~ 3 kbar shock accelerates toward the primary compaction front. When this pressure wave reaches the compaction front its amplitude rapidly decays due to the loss of the confinement of the compacted reactant. After these wave coalesce, a steady low velocity combustion wave propagates the remaining length of the granular bed at a speed of ~ 600 m/s. Solid volume fraction wave profiles are shown in Figure 3. Compaction waves with finite wave thickness of $\sim$ 2mm are supported by a small amount of solid-phase decomposition. Grain surface temperatures are calculated to be below the temperature needed to initiate grain burning.

Table 1. Thermophysical and Material Property Data

Variable [cgs units]	TS3659	WC140	HMX
d_p [μm]	434	411	100
ϕ_s°	0.6	0.6	0.73
ρ_s° [g/cm^3]	1.62	1.65	1.90
c_v^* [erg/g °K]	1.0×10^7	1.0×10^7	1.5×10^7
μ_c [g/cm^3 s]	$5.\times10^3$	$5.\times10^3$	$1.\times10^3$
T^* [°K]	460.	460.	550.
k_s [erg/g °K]	$1.\times10^4$	1×10^4	2.3×10^4
n	0.86	0.74	1.0
a [cm/s MPa^n]	0.247	0.306	0.123
b [s^{-1} MPa^{-2}]	0.012	0.022	0.018
ΔE_R [erg/g]	4.62×10^{10}	3.84×10^{10}	7.91×10^{10}
Q^* [erg/g]	0.4×10^{10}	0.4×10^{10}	0.4×10^{10}

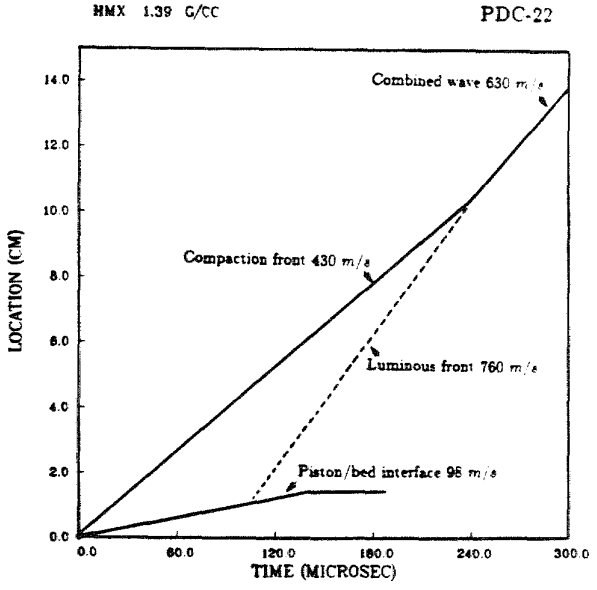

Figure 1. Distance-time experimental data for an impact of 98 m/s on 73% TMD HMX.

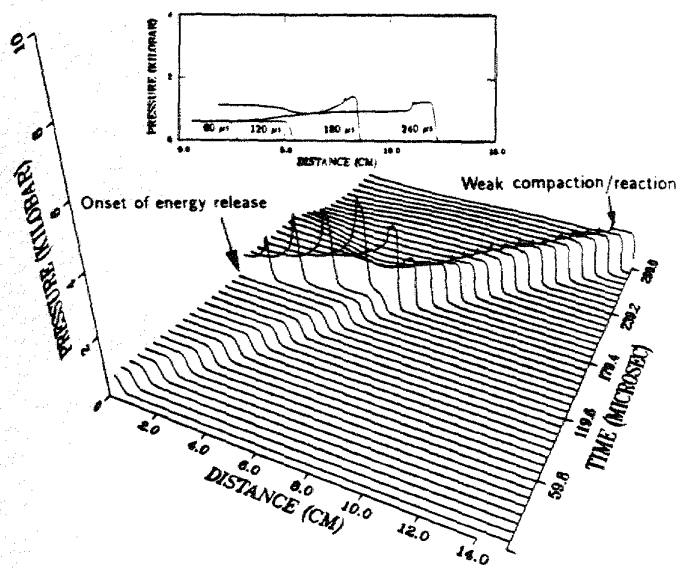

Figure 2. Calculated solid phase pressure profiles after impact at 98 m/s.

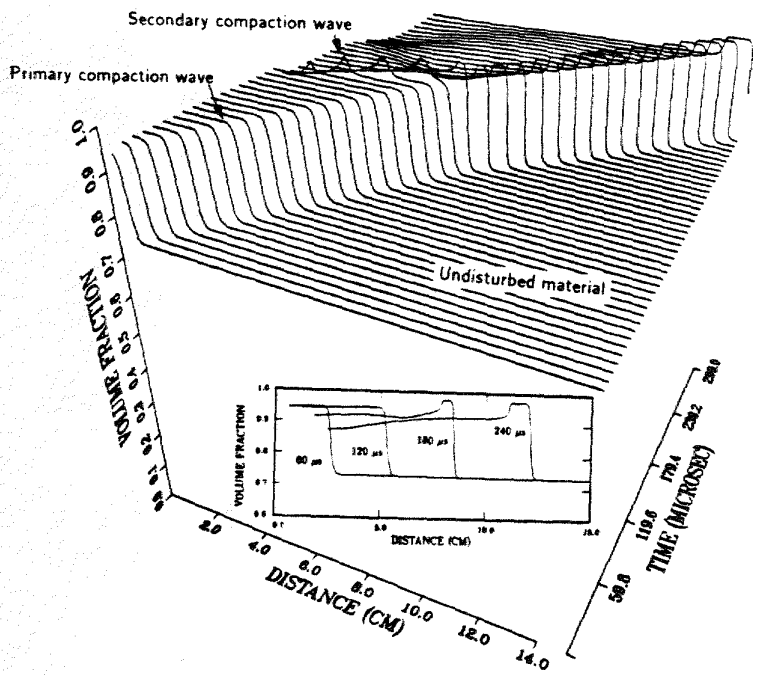

Figure 3. Solid phase volume fraction profiles after impact at 98 m/s.

At an impact velocity of 160 m/s, the compaction front is luminous, indicating the presence of 'hot-spot' decomposition very near the front as shown in Figure 4. Figure 5 displays the transient pressure wave profiles calculated for this impact condition. 'Hot-spot' initiation occurs quickly after impact and the ignition locus follows the compaction wave front. Initially, combustion assists the piston to produce a compaction wave with a speed of $\sim$ 800 m/s and, after 20 μs, grain surface temperatures indicates that grain burning is underway. Consistent with the experimental observation, grain burning occurs for a duration of $\sim$ 10μs, whereupon at a distance of 5 cm the transition to detonation takes place.

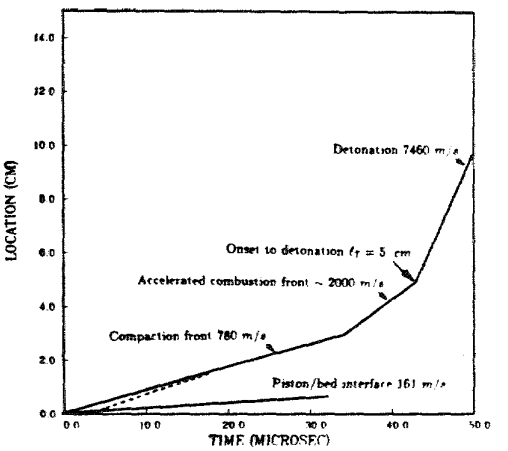

Figure 4. Distance-time experimental data for an impact of 161 m/s on 73% TMD HMX.

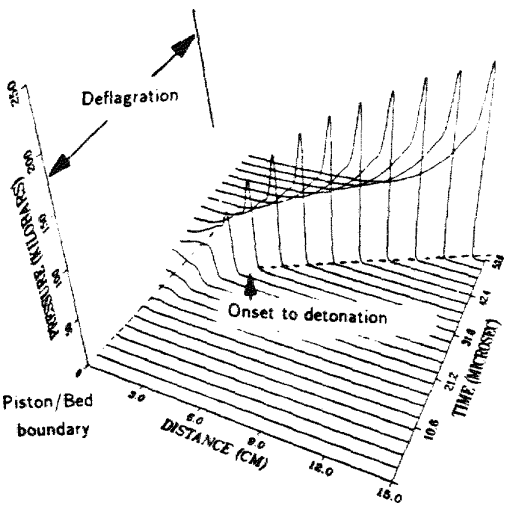

Figure 5. Solid phase pressure profiles after impact of 161 m/s.

In the series of experiments investigating dynamic compaction of nitrocellulose-based ball propellants, the reactive wave fields are probed using microwave interferometry. Wall pressure gauges provide additional information on the structure of the compaction and reactive pressure waves. In the calculations, wall pressures are estimated using the radial mixture stress defined by Kooker[29] incorporating the quasi-static axial and radial stress measurements of Campbell, et al.[30] Shown in Figure 6 are the distance-time trajectories of the waves induced by 192 m/s impact on 60% TMD TS3659. The compaction wave trajectory, measured by the microwave interferometry, is superimposed over the adaptive nodal meshing. In the adaptive calculations, closely-spaced nodal clusters indicate regions of high gradients, hence, the compaction and reactive waves can be clearly identified. As observed, piston impact produces a compaction wave that travels in the bed at 530 m/s. Following a delay of $\sim$ 200 μs, energy release in the 'hot-spot' reaction products within the 80% TMD compacted material supports a secondary wave that further compresses the reactant to total pore closure. Rapid heat transfer initiates grain burning and the two-phase combustion wave accelerates toward the primary compaction wave. Coalescence of the waves produces an abrupt change in the flame speed to $\sim$ 2000 m/s. (In this experiment the length of confinement was 10 cm so the merging of the reactive and compaction waves was not probed.) Included in these experiments are wall pressure gauges located at 3.81 and 7.62 cm from initial impact.

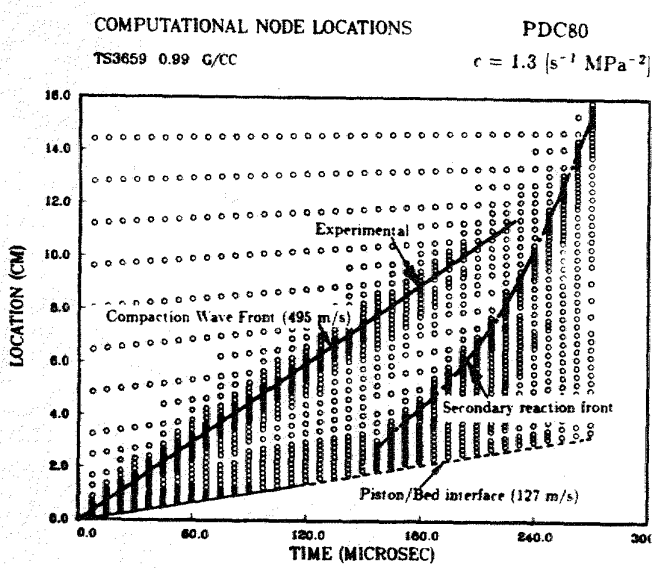

Figure 6. Transient variation of the computational nodes that follow compaction and reaction wave fronts. Overlayed is the observed compaction wave front for test PDC80.

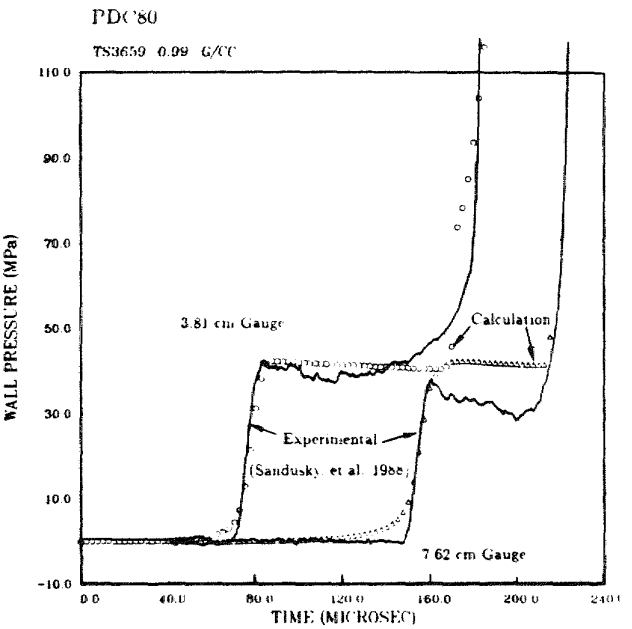

Figure 7. Comparison of calculated and measured wall pressures at 3.81 cm and 7.62 cm from impact in test PDC80.

Figure 7 shows a comparison of experimental and calculated wall pressures during dynamic compaction and combustion. As seen in this figure, predicted wall pressures are in reasonable agreement with experimental measurement. The slight drop in observed pressure following compaction is apparently due to the deceleration of the impacted piston.

Test PDC81 examines a higher impact condition on the double-based ball propellant TS3659 held in a steel confinement. Measurement of the transient piston velocity indicates significant piston deceleration after impact. The calculated and experimental wave trajectories are displayed in the adaptive node plot of Figure 8. For this case, impact produces a primary compaction wave with a speed of 530 m/s and after 180 μs, energy release triggers the secondary wave within the 90% TMD compacted material. When these waves coalesce, the reactive wave speed changes to $\sim$ 1800 m/s consistent with the microwave interferometric data. Figure 9 shows a comparison of calculated and measured wall stress. After 180 μs, rapid pressure growth occurs due to total pore closure ahead of the burn front. Figures 10 and 11 display the time and space evolution of mixture pressure and solid volume fraction for this loading condition. All wave features can be clearly identified.

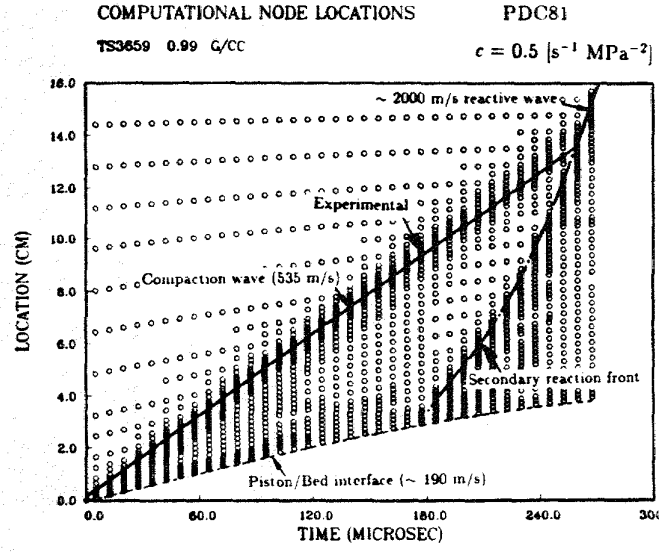

Figure 8. Wave trajectories followed by the adaptive nodes. Microwave interferometric data is overlayed for comparison. Note the abrupt change in wave speed at a time of ~ 240 μs.

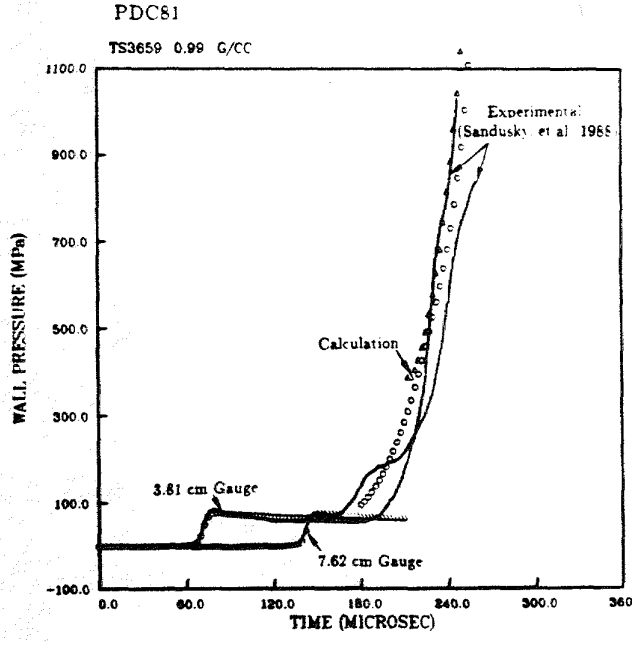

Figure 9. Comparison of calculated and measured wall pressures in test PDC81.

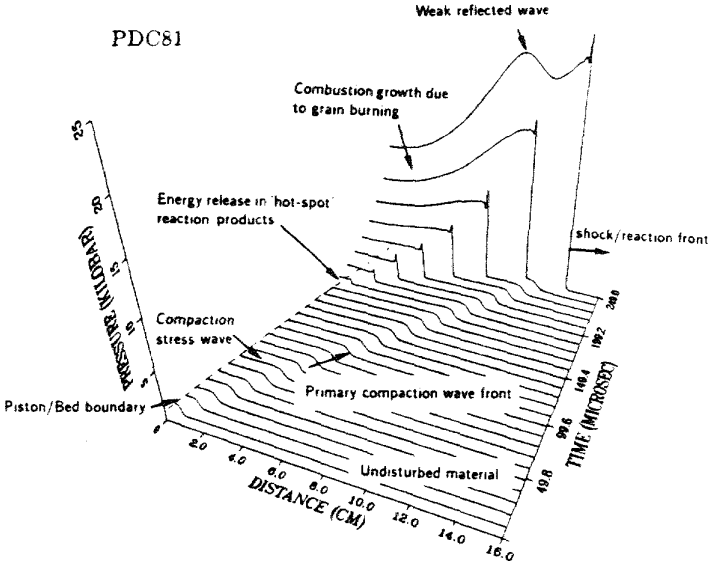

Figure 10. Calculated mixture pressure profiles after impact in TS3659 ball propellant in test PDC81.

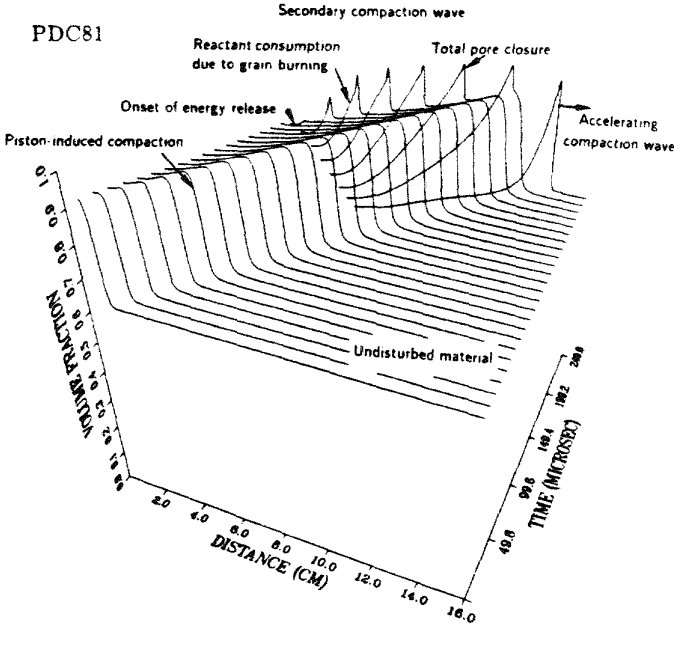

Figure 11. Calculated solid phase volume fraction profiles after impact in test PDC81. Note the development of the secondary compaction wave that produces total pore closure.

At a higher impact velocity of 216 m/s in test PDC82, piston impact produces compaction to 95% TMD and a deflagration front is promptly initiated leading to accelerated burning. Figure 12 displays the calculated and experimental wave trajectories. As experimentally observed, delayed reaction occurs 60 μs after impact and an accelerated combustion wave coalesces with the primary compaction wave at a distance 7 cm from initial impact at a time of $\sim$ 120 μs. The radial stress measurements and calculations are compared in Figure 13. Calculations indicate that energy release in the 'hot spot' decomposition products requires additional heatup time before the onset of grain burning seen as a 'plateau' in the pressure history of the 3.81 cm gauge.

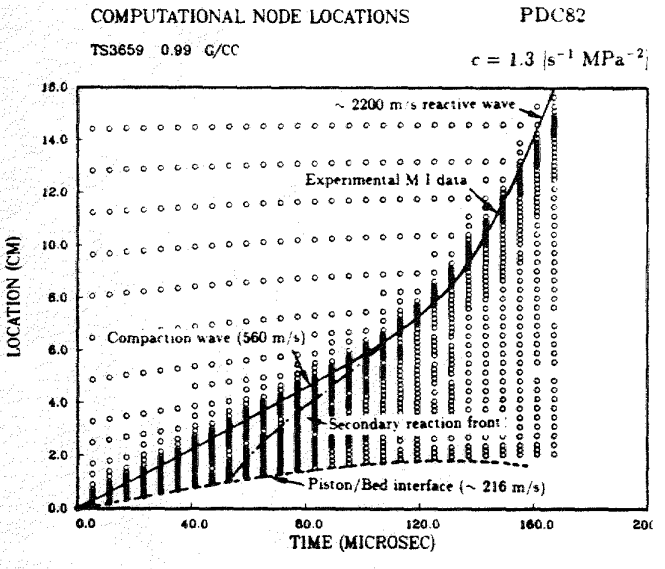

Figure 12. Wave trajectories followed by the adaptive nodes in test PDC82. Microwave interferometric data is superimposed.

In a piston impact experiment on 50% WC231, only wave trajectory information was obtained. All combustion and material property data were assumed to be equivalent to TS3659 with modification of particle size to d_p = 790 μm. Figure 14 shows the experimental waves observed for a 183 m/s impact condition. Calculation of this impact condition is shown in Figure 15 displaying the transient pressure wave profiles. For this case, a 85% TMD compaction wave evolves after impact and delayed energy release after $\sim$ 120 μs leads to a combustion event similar to that observed for TS3659. Merging of the waves produces a reactive shock wave that travels at a speed 1300 m/s.

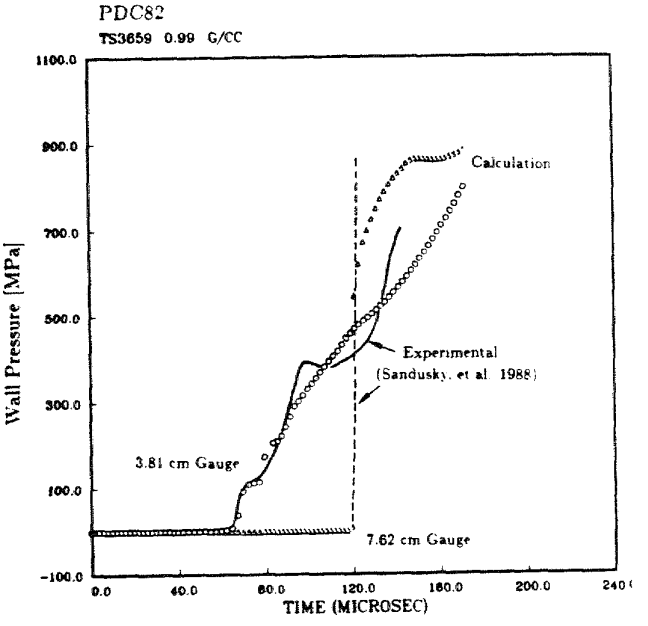

Figure 13. Comparison of calculated and measured wall pressures in test PDC82.

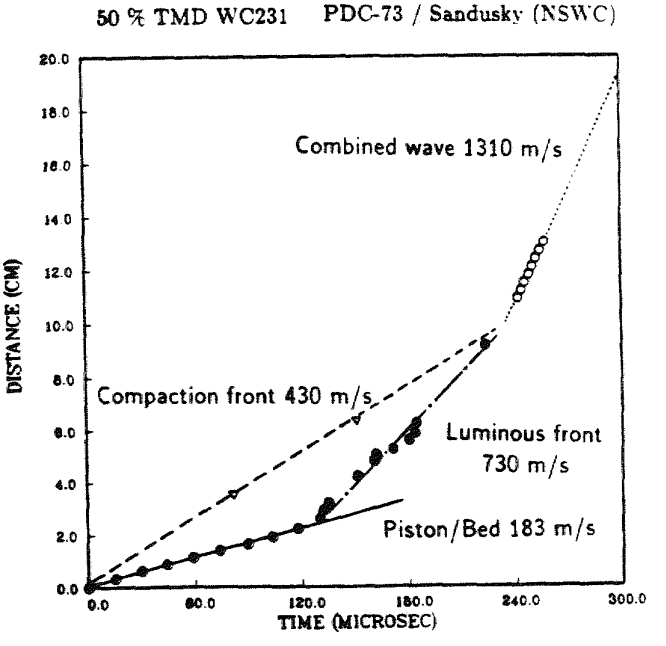

Figure 14. Distance-time trajectories of impact at 183 m/s on 50% TMD WC231.

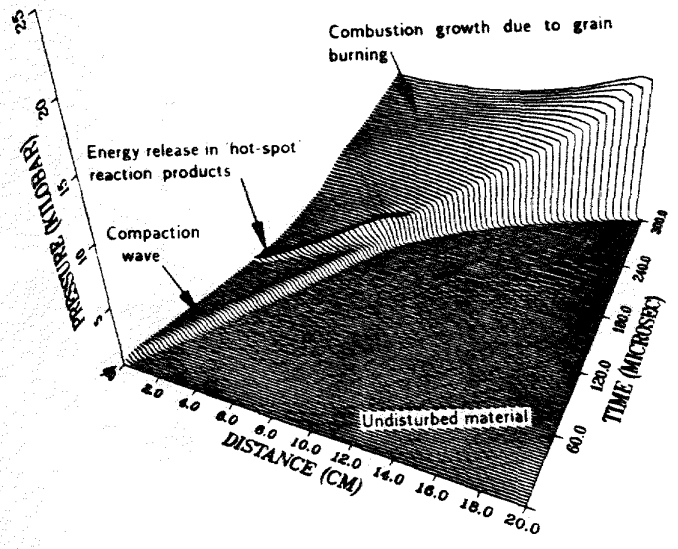

Figure 15. Calculated mixture pressure profiles for a 183 m/s impact on WC231.

Finally, impact of the single-based ball propellant WC140 designated as test M30 is considered. The first 100 μs of piston velocity were measured and piston deceleration was observed. The wave trajectories are shown in the adaptive node plot of Figure 16. After 240 μs, a secondary compaction/reaction wave appears and the microwave interferometry, monitoring the delayed wave, confirms a wave speed of ~ 1000 m/s consistent with that calculated. The wall pressure comparisons are shown in Figure 17. For this low impact condition, significant decay in wall pressure following compaction was observed prior to the onset of energy release. Although rarefaction is a result of deceleration of the piston, the unloading of the pressure within the compaction wave is greater than calculated. This behavior may be due to hysteresis of the loading vs. unloading intragranular stress that is not treated in the calculations. The reduced pressures during compaction appears to support the less reactive nature of WC140.

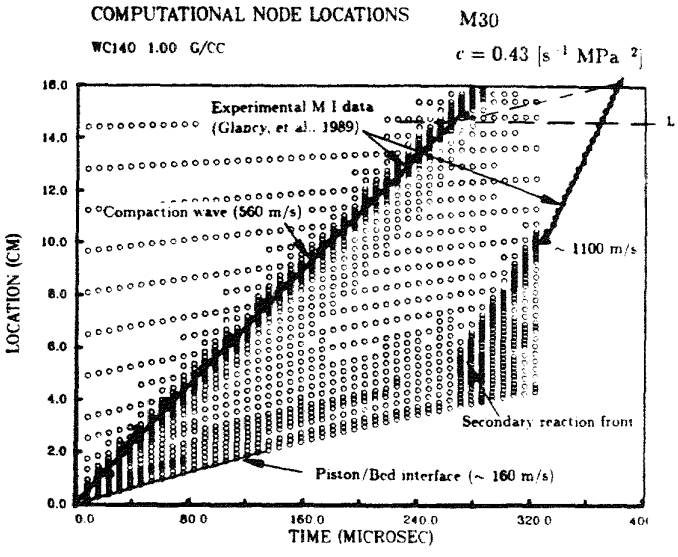

Figure 16. Wave trajectories followed by the adaptive nodes and the microwave interferometric data for impact on WC140. Note that the calculated secondary wave is consistent with experimental observation.

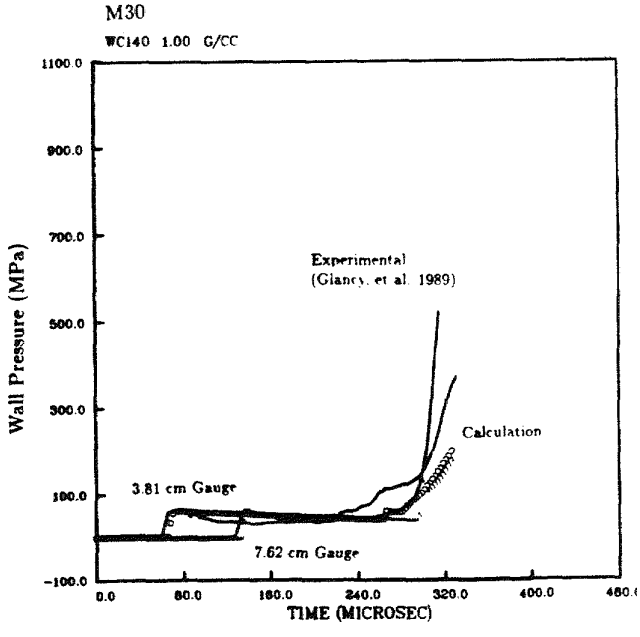

Figure 17. Comparison of calculated and measured wall pressures for a 160 m/s impact on WC140.

SUMMARY

This study has applied a multiphase flow description to treat the initiation and reactive growth of dynamically compacted granulated energetic materials. The multiphase reactive flow is described by a nonequilibrium continuum theory of mixtures formulated to include the compressibility of all phases and compaction behavior. A phenomenological model has been formulated within the context of the model to describe the 'hot-spot' thermal decomposition and grain burning.

As a general feature of the theoretical calculations, piston impact produces a shock-like compaction wave and a small fraction of the compacted reactant decomposes near the front. Subsequent energy release by the 'hot-spot' decomposition products triggers a pressure disturbance that supports a secondary compaction wave. Additional pore-collapse takes place (sometimes to total pore closure) and rapid pressurization occurs due to the confinement of the compacted reactant. With sufficient energy release and heat transfer, grain burning takes place within the compacted region whereupon high specific surface area of the granular reactant leads to rapid burning and the formation of compressive waves within the compacted reactant. A delayed reactive wave overtakes the primary compaction wave and combustion spreads rapidly into undisturbed material provided that inertial confinement of the unreacted material is sufficient to sustain accelerated combustion. Similar reaction/compaction wave behavior is described by Kooker's shock-wave model.[30]

Although the presented multiphase combustion model is sufficient to replicate the experimental data, this model is far from complete due to complex nature of the processes involved. More fundamental micromechanical and combustion models[31] are warranted. Clearly, better experimental insights into 'hot-spot' temperatures, number density distributions and volumes are required for detailed models of the compressive reaction induced by compaction.

Acknowledgment. — This work performed at Sandia National Laboratories supported by the U. S. Department of Energy under contract number DE-AC04-76DP00789.

REFERENCES

1. Bernecker, R. R., Sandusky, H. W. and Clairmont, A. R., "Deflagration-to-Detonation Transition Studies of Porous Explosive Charges in Plastic Tubes," *Seventh Symposium (International) on Detonation*, NSWC MP 82-334, pp 119-138, 1981.

2. Bernecker, R. R., Sandusky, H. W. and Clairmont, A. R., "Deflagration-to-Detonation Transition (DDT) Studies of a Double-Based Propellant," *Eighth Symposium (International) on Detonation*, NSWC MP 86-194, pp 658-668, 1985.

3. Green, L. G., James, E., Lee, E. L., Chambers, E. S., Tarver, C. M., Westmoreland, C., Weston, A. and Brown, B., "Delayed Detonation in Propellants from Low Velocity Impact", *Seventh Symposium (International) on Detonation*, NSWC MP 82-334, pp. 256-264, 1981.

4. Sandusky, H. W. and Bernecker, R. R., "Compressive Reaction in Porous Beds of Energetic Materials," *Eighth Symposium (International) on Detonation*, NSWC MP 86-194, pp 881-891, 1985.

5. Sandusky, H. W., Glancy, B. C., Campbell, R. L., Krall, A. D., Elban, W. L. and Coyne, P. J., "Compaction and Compressive Reaction Studies for a Spherical, Double-Base Ball Propellant" 1988 JANNAF Combustion Meeting, Huntsville, Ala. , October, 1988.

6. McAfee, J. M. and Campbell, A. W., "An Experimental Study of the Deflagration to Detonation Transition in Heavily Confined HMX," 1986 JANNAF Propulsion Systems Meeting, CPIA Pub. 446, Vol. I, pp. 163-186, 1986.

7. Baer, M. R. and Nunziato, J. W., "A Two-Phase Mixture Theory for Deflagration-to-Detonation Transition in Reactive Granular Materials," *Intl. J. Multiphase Flow*, **12**, pp 861-889, 1986.

8. Butler, P. B. and Krier, H., "Analysis of Deflagration-to-Detonation Transition in High-Energy Propellants", *Combustion and Flame*, **63**, pp 31-48, 1986.

9. Kooker, D. E. and Anderson, R. D. "A Mechanism for the Burning Rate of High Density, Porous Energetic Materials", *Seventh Symposium (International) on Detonation*, NSWC MP 82-334, pp. 198-215, 1981.

10. Kim, K., "Numerical Simulation of Convective Combustion of Ball Powders in Strong Confinement," *AIAA J.*, **22**, no. 6, pp 793-796, 1984.

11. *Eighth Symposium (International) on Detonation*, NSWC MP 86-194, 1985, see papers by Weston and Lee, Price and Boggs, and Verbeek.

12. Lee, E., Hornig, H. C. and Kury, J. W., "Adiabatic Expansion of High Explosive Detonation Products", LLNL UCRL-50422, Lawrence Livermore National Laboratory, 1968.

13. Sheffield, S. A., Mitchell, D. E. and Hayes, D. B., "An Equation of State and Chemical Kinetics for Hexanitrostilbene (HNS) Explosive", *Sixth Symposium (International) on Detonation*, ACR-221, pp 748-754, 1977.

14. Olinger, B., Roof, B. and Cady, H., "The Linear and Volume Compression of β-HMX and RDX to 9 GPa," LA-UR-78-1424, Los Alamos National Laboratory, 1978.

15. Verentennikov, V. A., Dremin, A. N., and Shvedov, K. K., "Shock Compressibility of NB Powder in the Porous and NonPorous States," *Fizika Goreniya I Vzryva*, **5**, no. 4, pp 499-505, 1969.

16. Elban, W. L. and Chiarito, M. A., "Quasi-Static Compaction Study of Coarse HMX Explosive," *Powder Technology*, **46**, pp 181-193, 1986.

17. Elban, W. L., "Quasi-Static Compaction Studies for DDT Investigations, Ball Propellants," *Propellants, Explosives & Pyrotechnics*, **9**, pp 119-129, 1984.

18. Sandusky, H. W. and Liddiard, T. P., "Dynamic Compaction of Porous Beds," NSWC TR-83-246, Naval Surface Weapons Center, 1985.

19. Boggs, T. L., "The Thermal Behavior of Cyclotrimethylenetrinitramine (RDX) and Cyclotetramethylenetetranitramine (HMX)," **Fundamentals of Solid-Propellant Combustion**, (ed. K. Kou and M. Summerfield), Progress in Astronautics and Aeronautics, **90**, pp 121-175, 1984.

20. Kooker, D. E., "A Workshop Summary of Model Predictions of the Piston-Driven-Compaction Experiment", 1989 JANNAF Propulsion Systems Hazards Meeting, San Antonio, Texas, Feb. 1989 (and references therein).

21. Dobratz, B. M., "LLNL Explosives Handbook: Properties of Chemical Explosives and Chemical Simulants," UCRL-52997, 1981

22. Fifer, R. A., "Chemistry of Nitrate Ester and Nitramine Propellants," **Fundamentals of Solid-Propellant Combustion**, (ed. K. Kou and M. Summerfield), Progress in Astronautics and Aeronautics, **90**, pp 177-237, 1984.

23. Baer, M. R., "A Model for Interface Temperature Induced by Convective Heat Transfer in Porous Materials," SAND88-1073, Sandia National Laboratories, 1989.

24. Baer, M. R., Benner, R. E., Gross, R. J., and Nunziato, J. W., "Modeling and Computation of Deflagration-to-Detonation Transition (DDT) in Reactive Granular Materials,"**Lectures in Applied Mathematics**, American Mathematical Society, **24**, pp. 479-498, 1986.

25. Verbeek, H. J., "Modeling of DDT in Granular Explosives," *Eighth Symposium (International) on Detonation*, NSWC MP 86-194, pp 669-677, 1985.

26. Embid, P. F. and Baer, M. R., "Mathematical Analysis of a Two-Phase Model for Reactive Granular Material," SAND88-3302, Sandia National Laboratories, 1989.

27. Baer, M. R., "Numerical Studies of Dynamic Compaction of Inert and Energetic Granular Materials," *J. of Applied Mechanics*, **55**, pp 36-43, 1988.

28. Kooker, D. E., "Predictions for the Piston-Driven Compaction Experiment Based on a Transient Shock Wave Model", 1989 JANNAF Propulsion Systems Hazards Meeting, San Antonio, Texas, Feb. 1989.

29. Campbell, R. L., Elban, W. L. and Coyne, P. J., "Side-Wall Pressure Measurements in Quasi-static Compaction of Porous Beds of HMX Powders and ABL 2523 Casting Powder," in Proceedings of 1988 Propulsion System Hazards Subcommittee Meeting, CPIA Publ. 477, Vol. I, 1988.

30. Kooker, D. E., "Collision of Reactive Compaction/Shock Waves in Granular Energetic Materials," in Proceeding of 1988 JANNAF Propulsion Systems Hazards Meeting, CPIA 477, Vol. I, pp 17-36, 1988.

31. Nunziato, J. W. and Baer, M. R., "A Microscopic Approach to the Initiation and Detonation of Condensed-Phase Energetic Mixtures", **Journal de Physique**, Colloque C4, no. 9, Tome 48, pp 67-83, September, 1987.